Structures 63 (2024) 106474

Contents lists available at ScienceDirect

Structures

journal homepage: www.elsevier.com/locate/structures

One-head masonry panels reinforced with industrial-waste fiber reinforced mortar: Investigating the effect of bed joints and coating reinforcement in the diagonal compressive behavior

Marco Vailati [a], Micaela Mercuri [b,*], Amedeo Gregori [a]

[a] Department of Civil, Construction-Architectural and Environmental Engineering, University of L'Aquila, Piazzale Ernesto Pontieri, Monteluco, 67100 L'Aquila, Poggio di Roio, Italy
[b] Department of Civil and Environmental Engineering, Northwestern University, Evanston, IL, USA

ARTICLE INFO

Keywords:
Seismic retrofitting
Bed-joints reinforcement
Glass fibers
Basalt fibers
External reinforcement
In-plane experimental test

ABSTRACT

Construction industry is a human activities that most contributes to the world pollution. Recent studies conducted by the EU Commission in 2019 highlighted that buildings and construction materials are responsible for 39% of the global emissions of carbon dioxide and 50% of the raw materials extraction, as well as one-third of the world's drinking water consumption. Analyzing the world of recycling mineral fibers, authors found that glass and basalt fibers from recycled waste, among other things, request less energy to obtain new filaments when compared to virgin fibers production. In this way, one can obtain a consistent reduction of energy consumption for building or retrofitting structures. In particular, authors explore in this study the benefits of using mineral fibers from recycled sources for strengthening brick masonry walls, carrying out diagonal compressive tests of one-head brick panels retrofiited with chopped fibers reinforced mortar. The aim of this study is twofold: understanding which type of chopped fibers is the most effective when dispersed in the mortar mix, i.e. basalt or glass fibers, and recognize the optimal location of the fiber reinforcement mortar with respect to the masonry panels. Under this perspective, three different set of panels are tested: (i) the reinforcing mortar is placed within the mortar joints of masonry panel; (ii) the reinforcing mortar is disposed as a double reinforcing layer on both the surfaces of the masonry panel, but the mortar joints are made out of plain mortar; (iii) the reinforcing mortar is placed both within the mortar joints of masonry bricks and as a double reinforcing layer on the surfaces of the masonry panel. Results are compared with reference panel made out of plain mortar and show that the most effective strengthening system is the one enriched by chopped basalt fibers. Generally, fiber reinforced mortar effectively strengthens both the loading and the post-peak capacity of the masonry panels, above all when used as coating layer on the external surfaces.

1. Introduction

Masonry buildings are prone to show diffusive damage phenomenon and collapse due to seismic actions. Recent earthquakes underlined the high vulnerability of these types of structures. Masonry structures can be classified into two main groups: (i) historical masonries, i.e. most of the world cultural heritage, being essentially composed by towers [1,2], palaces [3–5], and religious building [6–9], (ii) more recent masonries, hosting the majority of common people's houses in both undeveloped and industrialized countries [10]. In all these cases, having the perspective of minimizing human and economic losses, finding proper methods of analysis, verification procedures and, above all, effective strategies [11–14] for strengthening masonry systems is an urgent task for researchers, decision makers, engineering practitioner and all types of stakeholders.

During the last decades, two are the most widely diffused strengthening systems for masonry structures: fiber reinforced polymers (FRP) [15–21] and fiber reinforced cementitious matrix (FRCM) composites [22–28]. FRPs are characterized by several advantages, such as low specific weight, corrosion resistance, high tensile strength, and adaptability to curved surfaces [29–45]. On the other hand, they show non negligible disadvantages, such as low fire resistance, low permeability, impossibility of application on wet surfaces and no satisfactory chemical compatibility with masonry supports, that makes them inadequate for

* Corresponding author.
E-mail address: micaela.mercuri@northwetsern.edu (M. Mercuri).

https://doi.org/10.1016/j.istruc.2024.106474
Received 3 January 2024; Received in revised form 2 April 2024; Accepted 22 April 2024
Available online 6 May 2024

restoration works on cultural heritage architectures.

FRCM's are nowadays the favorite in plane and out-of-plane retrofitting systems for masonry structures [46–60], because of their intrinsic sustainability and for the beneficial effects related to their good resistance to high temperatures and vapor permeability [61]. FRCM's are generally composed by fiber fabrics coupled with a mortar characterized by an inorganic matrix. The textile component provides the use of fiber made out of steel [62–65], carbon [66–69], glass [70–73], basalt [74–78], aramid [79] and also vegetable fibers [80–82]. The main FRCM drawback arises when these materials are applied on large-scale structural masonry systems: the installation procedure, being almost hand-made and very time consuming, becomes most of times a very difficult and unfeasible alternative. As a matter of fact, the process related to FRCM application consists of at least three phases, i.e. (i) application of the mortar matrix on the masonry surface, as a first and thin layer; (ii) installation of the fiber grid reinforcement by mean of a light pressure on the first layer of fresh mortar; (iii) drafting of the second and finishing layer of mortar, fully covering the grid and totally embedding the fibers into the inorganic matrix of mortar.

The aim of this paper is to propose an innovative mortar, a fiber reinforced mortar (denominated hereinafter FRM), reinforced with chopped fibers directly mixed within the mortar matrix, for an extensive and expeditious strengthening of new and existing masonry structures. The main characteristic of the proposed mortar is that it can be applied as a single layer and all at once on the masonry support, being sprayed or manually spread on the panel. For this reason, the newly proposed mortar becomes very attractive both under the practical and the economical perspectives, as the repair costs and constructions times decrease and labor jobs are facilitated.

In particular, this study investigates the effect of both glass fiber reinforced mortars (GFRM) and basalt fiber reinforced mortars (BFRM) on the diagonal shear behavior of one-head brick masonry panels in the three following configurations: (i) the reinforced mortar is placed within the mortar joints of masonry panel; (ii) the reinforcing mortar is disposed as a double reinforcing layer on both the surfaces of the masonry panel, but the mortar joints are made out of plain mortar; (iii) the reinforcing mortar is placed both within the mortar joints of masonry bricks and as a double reinforcing layer on the surfaces of the masonry panel.

2. Materials and methods

This section reports the mechanical properties of the elementary materials, i.e. the masonry bricks (Section 2.1) and the plain mortar (Section 2.2.1) composing the one-head masonry panel. Immediately after, both the geometrical and mechanical properties of chopped glass fibers and basalt fibers are shown, and both reinforced mortars (Glass FRM and Basalt FRM) are characterized in terms of flexural, tensile and compressive capacity (Section 2.2.2).

2.1. Bricks

Standard tests according to [83] are performed on masonry bricks to calculate their fundamental properties. The results of the bricks characterization are reported in Table 1. The coefficients of variation reported in Table 1 were computed after testing 15 bricks.

Table 1
Geometrical properties and mechanical characterization of masonry bricks. The Coefficient of Variation is reported between parenthesis in the right column.

Property	Value (CoV in %)
Dimension (mm)	240 ×120 x 55 (1)
Compressive strength (MPa)	35 (7)
Tensile strength (MPa)	3.7 (5)
Water absorption (%)	14.8 (9)

2.2. Mortar

Three different mortars are used in this study to investigate their effect on the mechanical behavior of one-head masonry panel: (i) plain mortar, (ii) chopped glass reinforced mortar, (iii) chopped basalt fiber reinforced mortar. It is important underlying that, as the aim of this paper is to analyze the effect of the two different types of fiber on the mechanical properties of the masonry wall, the mortar mix design, as well as the water content was kept fixed for both unreinforced and reinforced mortars.

2.2.1. Unreinforced mortar

The mix-design used for the preparation of all the samples are characterized by aggregates composed by sand, whose size goes from 0.1 mm to 1.2 mm and whose content is equal to 65% of the total weight of the mixture. In terms of binders, the lime content is the 70% of the total weight of the binder, and the remaining 30% is a Portland cementitious binder. It is worth underlying that the weight of the binder is 33% of the total weight of the mixture. The adopted water content corresponds to the 8% of the weight of the binder and to the 2% of the total weight of the product. After the mix-phase, the mortar was cast in three molds measuring 160 mm in length, 40 mm in height and 40 mm in depth and the drying phase started. After 28 days the specimens were tested according to the standard code EN 1015–11 [84], in flexural configuration. For the characterization of the tensile and the compressive response, the tests were performed on 40 mm × 40 mm x 80 mm prisms obtained from one the two-half specimens representing the broken pieces of the three-point bending test (3PBT). Fig. 1 illustrates the testing apparatus and structural schemes for 3PBT, the splitting test (ST), and the compression test (CT).

After having performed the 3PBT, the flexural strength is computed by means of $\sigma_f = \frac{3VL}{2b(d-a)^2}$.In this equation, V is the peak vertical load, b is the depth of the specimen, d is its height, a is the crack length and L is the specimen length.

From the ST and the CT, the tensile strength f_t and the compressive strength f_c can be computed, resorting on $f_t = \frac{2F}{\pi bd}$ and $f_c = \frac{C}{bL_2}$, respectively. In these equations, F and C are the peak vertical loads in tensile and compressive configuration, respectively.

For the three plain mortar cases (URM), as well as for the three GFRM cases and the three BFRM cases, Fig. 3a and b show the flexural stress σ_f and tensile stress $f_t$versus displacement δ curves, respectively. Fig. 3c reports the compressive stress f_c versus vertical strain ε_v for the same aforementioned cases.

2.2.2. Reinforced mortar: glass FRM and Basalt FRM

The first step in this subsection is to illustrate both the geometrical and mechanical properties of both glass and basal fibers, that are exhaustively reported in Table 2 and Fig. 2. In Table 2, l_f is the fiber length, d_f is the diameter of each yearn, ρ_f is fiber density, E_f is fiber Young's modulus, E_f is fiber Young's modulus, $f_{t,f}$ is the tensile strength, $\varepsilon_{u,f}$ is the fiber ultimate strain. It is important to underline that the geometrical characteristics of the two fiber types are chosen as close as possible, aiming to investigate just the mechanical effect of the fiber type on the diagonal behavior of the one-head brick panel. The difference between plain mortar and fiber reinforced samples is that, in the latter case, fibers are included within the mortar mix: they are mixed to the dried mixture as last step before the addition of water in the conglomerate.

It is also fundamental to report here the procedure followed for the determination of the fiber content (FC) to be incorporated within the dry-mixing phase. Several recent studies pointed out that all the mechanical properties of fiber reinforced mortar enhance while augmenting the fiber content, while keeping constant the fiber length [85]. From

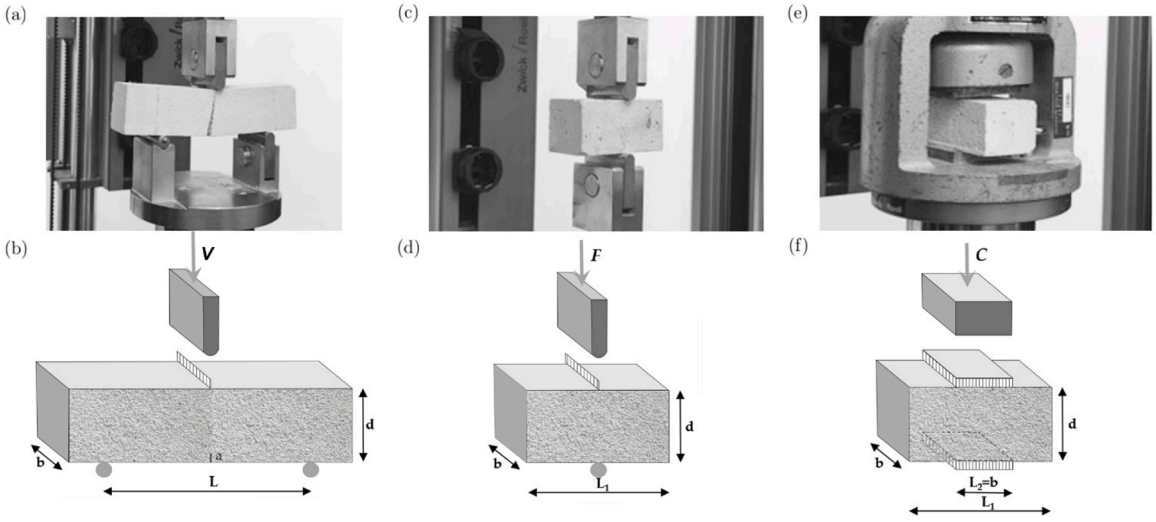

Fig. 1. Experimental apparatus for the mechanical characterization of the mortar: a) and b) three-point bending test (3PBT), c) and d) splitting test (ST), e) and f) compression test (CT).

Fig. 2. (left) Glass fibers; (right) Basalt fibers.

this statement, one can wrongly deduce that the optimal fiber content is the maximum one. Nevertheless, this is not the best engineering solution because it does not account for rheological requirements, denoted by the workability. The workability is a fundamental property when a considering to apply a conglomerate on a large scale, for structural purposes and by both ordinary and specialized workmanship. It is considered that the workability requirement is satisfied if the slump value is not less that 15.5 mm. This value is met for a fiber content FC= 1.2% for glass fiber reinforced mortar and FC= 1.9% for basalt fiber reinforced mortar. It is worth underlying that, for conglomerate without the addition of fibers, the slump value was 19 mm, much greater than the fiber added conglomerates. Therefore, the addition of fibers in the mortar decreases its workability.

To mechanically characterize both the glass and basalt reinforced mortars, the same procedure adopted for the unreinforced mortar (previously reported in Section 2.2.1) was followed. The inferred flexural, tensile, compressive properties are reported in Fig. 3a, b, and c, respectively. In Fig. 3, the light orange, the dark orange and the gray continuous lines denotes mechanical behaviors related to GFRM, BFRM

Table 2
Geometrical and mechanical properties of the glass and basalt fibers dispersed in the mortar matrix. l_f is the fiber length, d_f is the diameter of each yearn, ρ_f is fiber density, E_f is fiber Young's modulus, E_f is fiber Young's modulus, $f_{t,f}$ is the tensile strength, $\varepsilon_{u,f}$ is the fiber ultimate strain.

Nomenclature	l_f (mm)	d_f (mm)	ρ_f (kg/m^3)	E_f (MPa)	$f_{t,f}$ (MPa)	$\varepsilon_{u,f}$ (%)
Glass F12	12	0.0135	2680	72,000	1700	3.7
Basalt F12	12	0.04	1300	41,000	1600	6.5

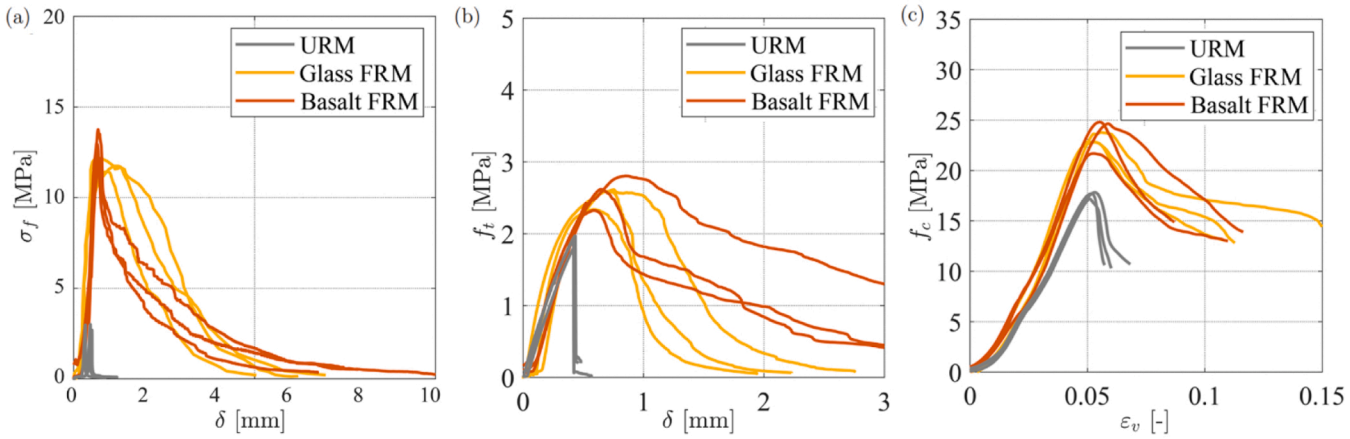

Fig. 3. a) Flexural stress σ_f vs displacement δ curves; b) Tensile stress f_t vs displacement δ curves; c) Compressive stress f_c vs vertical strain ε_v curves.

and URM, respectively. In particular, Fig. 3a and b show the flexural stress σ_f and tensile stress $f_t$versus displacement δ curves, respectively, for both GFRM and BFRM. For the same cases, Fig. 3c illustrates the compressive stress f_c versus vertical strain ε_v. Table 3 reports the flexural strength σ_f, the tensile strength f_t, the compressive strength f_c of plain mortar and reinforced mortars, i.e. GFRM and BFRM, together with their coefficients of variation in parenthesis (CoV). It is interesting to notice that the most beneficial effect provided by both the glass and basalt fibers is in favor of the flexural behavior, rather than the tensile or compressive ones. The underlined physical reason can be plausibly traced in the modality of failure. The flexural behavior provides the fracture to propagate along the ligament while encountering fibers and, in this case, the observed rupture mechanism is essentially governed by sliding between fibers and surrounding mortar. On the other hand, in compression and tension, fibers modestly increase the strength because they fiber break without sliding with respect to the surrounding mortar.

2.3. Experimental design

The aim of the experimental campaign is twofold: understanding what mortar between the glass fiber reinforced and the basalt fiber reinforced is the most effective in improving the compressive-shear behavior of one-head masonry panel; inferring what is the best location of reinforced mortar with respect to the masonry panel. For this latter reason, three different arrangement of the reinforced mortar are designed: (i) FRMs placed just in the mortar joints, (ii) unreinforced mortar joints and FRMs arranged as an internal-external layer on the surface of the masonry panel, and (ii) FRMs placed in both mortar joints and an as an internal-external layer on the surface of the masonry panels. Fig. 4 shows the scheme of all the tested cases.

For the listed aims of this study, one panel with joints characterized by plain mortar and denominated URM in Table 3 is also tested. Obviously, this test corresponds to the unreinforced case. The three different configurations are analyzed for both the glass fiber reinforcement and the basalt fiber reinforcement. Let's browse the three sets of cases. The first set is characterized by masonry panels measuring 990 mm × 965 mm x 120 mm and they have a joint-mortar-thickness equal to 10 mm. The joints can be either reinforced by glass fiber mortar of by basalt fiber one. These cases are named J-G_{FRM} and J-B_{FRM} cases in Table 4 and they are shown in Fig. 5a. The second set of experiments is composed by panels measuring 990 mm × 965 mm x 160 mm. For these panels, the joints are characterized by unreinforced mortar, whereas the out of plane dimension includes a 20 mm thickness coating (a total of 40 mm as the coating is on both the internal and external surfaces), with either glass fiber mortar (C-G_{FRM} case in Table 4) or basalt fiber mortar (C-B_{FRM} case in Table 4). For the sake of comparison, a panel with unreinforced mortar placed in both the joints and external coating is tested and named C_{URM} in Table 4. The third and last set of panels have both reinforced joints and coating with either glass or basalt fibers and they are denominated JC-G_{FRM} and JC-B_{FRM} in Table 4, respectively. It is important underlying that in all the C-cases, reinforced mortar is applied just on the two external surfaces and, for this reason, the proposed reinforcement system is suitable to strengthen both existing and newly built. On the other hand, all the J-cases provide the entire reinforcement of the mortar joints with fibers and the reinforcement system is therefore applicable just to new constructions.

Table 3
Mechanical properties of plain mortar and reinforced mortars, i.e. GFRM and BFRM.

Nomenclature	σ_f [MPa] (CoV in %)	f_t [MPa] (CoV in %)	f_c [MPa] (CoV in %)
Plain mortar prisms	2.9 (6.1)	1.9(2.6)	17.5 (1.8)
Glass FRM prisms	11.7 (6.4)	2.4 (3.2)	23.8 (4.2)
Basalt FRM prisms	12.1 (7.4)	2.6 (9.6)	24.1 (6.0)

2.4. Test setup and loading protocol

ASTM E519/E519M-21 details the test apparatus and loading protocol adopted in this study [75]. It is worth underlying that all panels were preliminarily rotated of 45° with respect to the horizontal axis and collocated in the Instron machine in Laboratory of Material and Structures of University of L'Aquila (IST Systems - Labtronic 8800 Structural Test Controls System), as shown in Fig. 5b. Fig. 5c shows the experimental setup for the diagonal compression test and it underlies some details of the loading apparatus: a couple o 'V-shaped' steel elements measuring about 152 mm each side, were placed at the two panel corners and connected by two triangular steel plates, aiming to avoid the crushing-corner modality of failure. Two Linear Variable Displacement Transducers (LVDTs) are placed on each side of the panel (for a total of four transducers) to record both vertical and horizontal panel displacements. The LVDTs base length was kept constant at about 800 mm. The force was applied in displacement control conditions on the top of the vertical axis of the panel, whereas the bottom side was fixed in translations and rotations. The loading rate was about 0.5 mm/min and the piston advanced up to the complete sample failure. Data points related to both loads and displacements were recorded at a frequency equal to 5 Hz.

3. Analysis of results

3.1. Improvement of the bearing capacity

Fig. 6 shows the experimental results for the three set of cases. More precisely, Fig. 6a reports the vertical load P versus vertical displacements Δv curves for the set of cases with fiber reinforced joints; Fig. 6b shows the same curves for the set of cases with fiber reinforced mortar applied as external layer coating; Fig. 6c depicts the P - Δv curves for the set of cases characterized by both fiber reinforced mortar joints and coating layers. From the comparison between the URM case and the J-G_{FRM} and J-B_{FRM} cases in Fig. 6a, it appears clear the beneficial effect of the chopped fibers when used as a reinforcement for mortar joints. In fact, the peak loads related to J-B_{FRM} and J-G_{FRM} cases increase of 66.7% and 48.2% with respect to the URM case, respectively. By comparing the URM case and the C-G_{FRM} and C-B_{FRM} cases in Fig. 6b, it is also evident that using chopped fibers in the coating mortar enhances the load bearing capacity of one-head brick panels. In fact, the peak loads related to C-B_{FRM} and C-G_{FRM} cases increase of 266.7% and 159.3% with respect to the URM case, respectively. For this set of cases, it is of paramount importance the comparison with the C_{URM} case. In this case, the peak loads related to C-B_{FRM} and C-G_{FRM} cases increase of 132.6% and 62.8% with respect to the C_{URM} case, respectively. The combined effect of reinforced mortar within the mortar joints and as superficial coating leads to the maximum improvement of the bearing capacity, as shown in Fig. 6c. In this case, the peak loads related to JC-B_{FRM} and JC-G_{FRM} cases increase of 366.7% and 307.4% with respect to the URM case, respectively. Additionally, the peak loads related to JC-B_{FRM} and JC-G_{FRM} cases increase of 193% and 155.8% with respect to the C_{URM} case, respectively. As additional general result, it is important underlying that, for all the analyzed set of cases, the beneficial effect of the reinforced mortar is more pronounced when chopped basalt fibers are used with respect to the glass fiber cases.

3.1.1. Shear strength

According to the ASTM E519/E519M-21 [86,87] it is possible to compute the shear stress τ resorting on the following equation:

$$\tau = \frac{0.707P}{A_n} \quad (1)$$

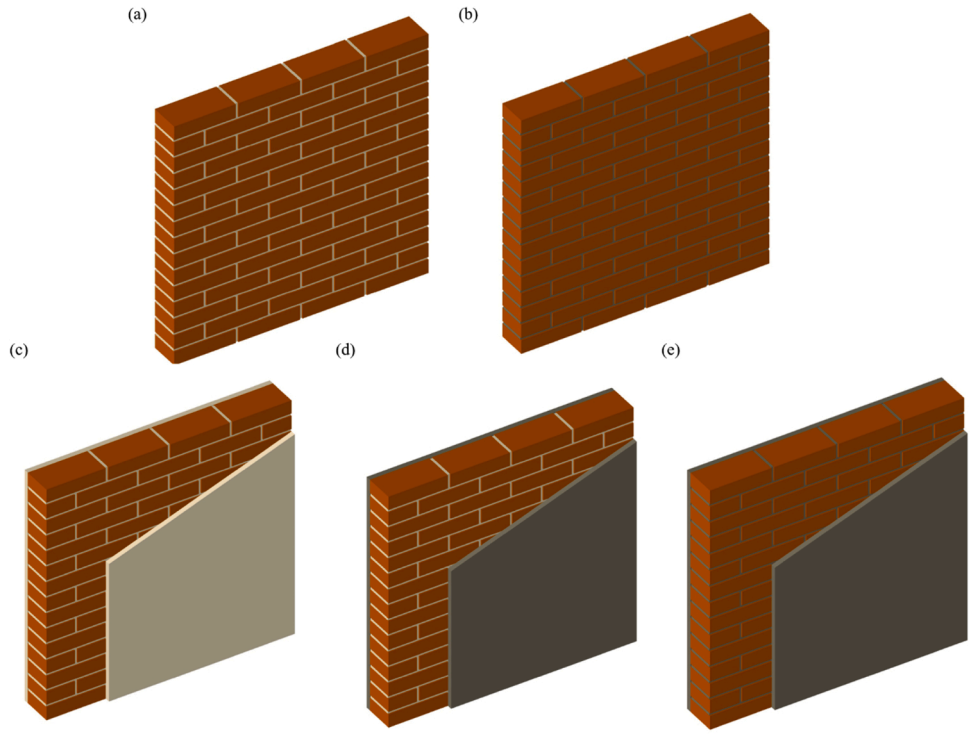

Fig. 4. (a) URM case: plain mortar placed in joints; (b) J-cases: FRM placed in mortar joints; (c) C_{URM}: plain mortar placed in mortar joints and as external coating; (d) C-cases: plain mortar joints placed in joints and FRM placed as external coating; (e) JC-cases: FRM placed in joints and as external coating.

Table 4
Summary of brick masonry panels tested in diagonal-compressive configuration.

Nomenclature	Dimensions (mm)	Joint Reinforcement type	External Reinforcement type
URM	990 × 965 x 120	-	-
J-G_{FRM}	990 × 965 x 120	Glass fibers	-
J-B_{FRM}	990 × 965 x 120	Basalt fibers	-
C_{URM}	990 × 965 x 160	-	-
C-G_{FRM}	990 × 965 x 160	-	Glass fibers
C-B_{FRM}	990 × 965 x 160	-	Basalt fibers
JC-G_{FRM}	990 × 965 x 160	Glass fibers	Glass fibers
JC-B_{FRM}	990 × 965 x 160	Basalt fibers	Basalt fibers

Where A_n is net area of the panel expressed as $A_n = (W+h)/2) * t$ and W, h, t and n are the width, height, and thickness of the panel. When P reaches P_0, τ reaches the shear strength τ_0. To compute the deformation capacity of the panel, one can write the following equation:

$$\gamma = \frac{\Delta v + \Delta h}{g} \tag{2}$$

where Δv and Δh are the vertical and horizontal displacements measured by the LVDTs and g is the LVDT length.

The results are shown in Fig. 7, that reports the shear stress τ versus shear strain γ curves. The same qualitative results pointed out on the P versus Δv curves shown in Fig. 6 appear in Fig. 7 and they are related to the shearing capacity of the panels. It is important to express the shear capacity of each set of cases, because their effective transversal area is different: J cases do not have the contribution of the coating on A_n, whereas all the other cases do have. For all the three set of cases, the fiber beneficial effect is more evident when basalt fibers are used with respect to glass fibers (comparison of red and blue curves in Fig. 7). When fibers are used in the mortar joints (J-G_{FRM} and J-B_{FRM} cases in Fig. 7a) the beneficial effect is moderate and the shear strength related to J-B_{FRM} and J-G_{FRM} cases increase of 66.7% and 48.2% than to the URM case, respectively.

When fiber reinforced mortar is used as a double layer reinforcing (C-B_{FRM} and C-G_{FRM} cases in Fig. 7b), the shear strengths increase of 248.6% and 128.6% with respect to URM case, respectively. More importantly, the shear strengths increase of 144% and 60% with respect to C_{URM} case, respectively. The optimum solution in reached when fiber reinforced mortar is used both within the joints and as an internal-external coating (JC-B_{FRM} and JC-G_{FRM} cases in Fig. 7c): in this cases the shear strengths increase of 328.6% and 285.7% with respect to URM case, respectively. When compared with the C_{URM} case, the shear strengths augments of 200% and 170% for JC-B_{FRM} and JC-G_{FRM} cases, respectively.

3.1.2. *Shear modulus and Young's modulus*

Few considerations can be done after computing the Shear Modulus G for each panels and the Young's Modulus E, resorting to the formula $E = 2G(1 + \nu)$, where ν is the Poisson's coefficient, taken as 0.25 for beick masonry walls. The addition of fibers in the joints does not seem to enhance the panel's stiffness, that is instead slightly decreasing. On the other hand, the fiber effect in the coating increases the panel's stiffness. This effect is moe pronounced when fibers are reinforcing mortar in both joints and panel surfaces. All these considerations are shown in Table 5. However, it is worth noting that both G and E varies about 15–20%, that is considered a values within the scattering of experimental data for URM and fiber reinforced masonry.

3.2. *Improvement of the post-peak capacity*

The aim of Section 3.1 was to point out the enhancement of the diagonal and shear bearing capacity by means of the use of fiber reinforced

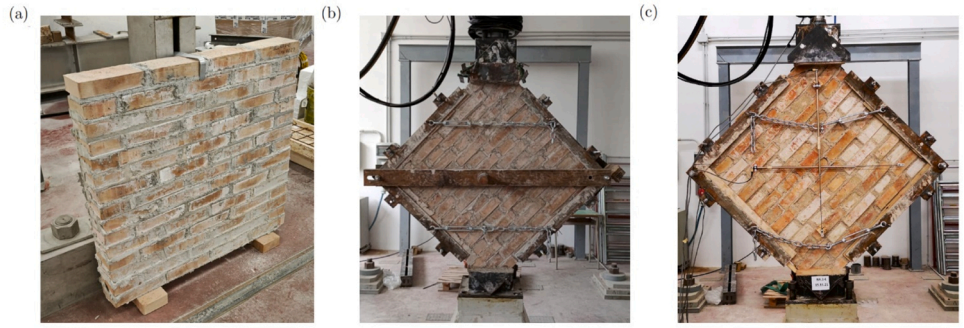

Fig. 5. (a) Preparation of the one-head brick masonry panel (J-B_{FRM}); (b) the panel is rotated of 45° with respect to the horizontal axis and placed on the Instron machine in Laboratory of Material and Structures of University of L'Aquila; c) two Linear Variable Displacement Transducers (LVDTs) are collocated on each side, being able to measure the vertical and horizontal displacements.

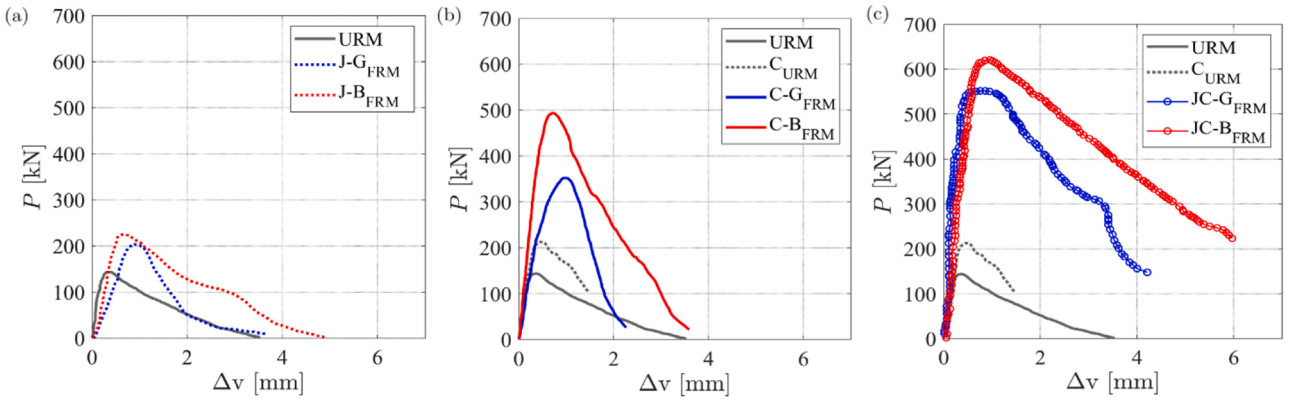

Fig. 6. Load P versus vertical displacements Δv curves for cases with reinforced mortar placed in: (a) mortar joints; (b) as internal-external coating; (c) both mortar joints and internal-external coating; in gray is also reported the unreinforced case (URM).

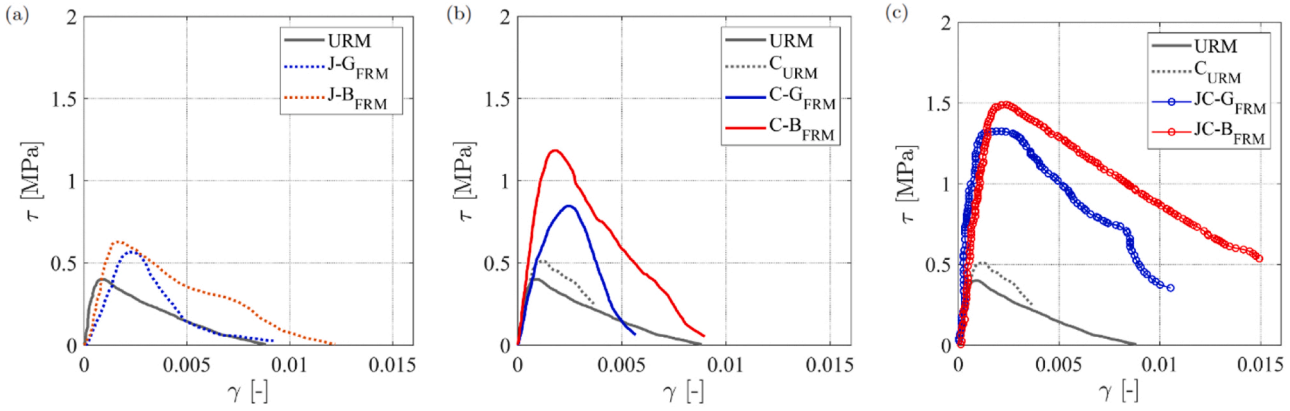

Fig. 7. Shear stress τ versus shear strain γ curves for cases with reinforced mortar placed in: (a) mortar joints; (b) as internal-external coating; (c) both mortar joints and internal-external coating; in gray is also reported the unreinforced case (URM).

Table 5
Shear modulus, Young's modulus for all the tested masonry panels.

Nomenclature	Shear Modulus G [MPa]	Young's Modulus E [MPa]
URM	2666.7	6666.8
J-G_{FRM}	2500.0	6250.0
J-B_{FRM}	2353.0	5882.4
C_{URM}	2857.0	7143.8
C-G_{FRM}	2862.0	7155.0
C-B_{FRM}	2898.0	7246.4
JC-G_{FRM}	3076.0	7690.0
JC-B_{FRM}	2963.0	7407.4

mortar. The current section demonstrates the improvement of the post-peak capacity of one-head brick masonry panels under the qualitative point of view, by means of the fracture propagation pattern, and under the quantitative perspective, through the calculation of the pseudo-ductility.

3.2.1. *Fracture propagation phenomenon*

The modality of fracture propagation has necessarily repercussions on the post-peak capacity for all quasi-brittle materials and, particularly, for masonry walls. As the fracture advances, the energy released during the fracture propagation increases. The more articulated and extended is

the fracturing pattern, the greater is the energy dissipated in the nonlinear regime. Fig. 8 shows the comparison between different fracturing patterns related to: the unreinforced case (Fig. 8a), the fiber reinforced mortar joint cases (J-G_{FRM} and J-B_{FRM} cases in Fig. 8b), the reinforced mortar used as external coating (C-B_{FRM} and C-G_{FRM} cases in Fig. 8c), and fiber reinforced mortar used within panel joints and external coating surface (JC-B_{FRM} and JC-G_{FRM} cases in Fig. 8d). Interesting observation can be pointed out: when mortar joints are made out of plain mortar, the fracture is located within the joints and at the brick-mortar interface; if mortar joints are reinforced with fibers, joints resistance to fracture because of the presence of chopped fibers and fracture is more articulated and located in the mortar joints, in the brick-mortar interface and, above all, it can happen within the masonry brick. This phenomenon justifies the enhancement of the post peak capacity for the J-G_{FRM} and J-B_{FRM} cases in Figs. 7a and 8b. In the second set of cases, i.e. when the reinforcing mortar is used as superficial coating (C-G_{FRM} and C-B_{FRM} cases in Figs. 7b and 8c), the fracturing pattern is more marked oriented in the vertical and is less articulated spatially. From this observation, one can infer that the responsibility for increasing the post-peak capacity is due to the mortar coating, whose effect is predominant with respect to the brick-joint sublayer. The last instructive fracturing patterns are related to JC-G_{FRM} and JC-B_{FRM} cases, depicted in Figs. 7c and 8d: for these panels, there is not a single macro crack, but the coalescence of multiple meso- and micro-cracks, all oriented in the vertical direction. This observation suggests the presence of two antagonists structural element, i.e. the brick-mortar substrate and the coating layer, that are competing for the post-peak loading capacity: the joints reinforcement directs the fracture within the brick-mortar interface, whereas the superficial reinforcement orients the single crack in the vertical direction. The overall results can be seen as a superposition of both the strengthening effects.

3.2.2. Pseudo-ductility

To quantify the enhancement of the post-peak capacity under a quantitative point of view, we calculated the pseudo-ductility for all the different set of cases [88]. Generally, it is very important resorting on the structural ductility and this feature is also quantitatively considered by many seismic based design codes [89,90]. For the purposes of this study, the pseudo-ductility was determined resorting on an equivalent elasto-perfectly plastic constitutive behavior, as the shear stress-strain plots did not show a distinct yield point: (i) for the ultimate strain γ_u the shear strain correspondent to a shear strength degraded to $0.8\tau_0$ was considered; (ii) the yield strain γ_y the shear strain was determined such that the area under the bilinear curve was coincident with the experimental one. Then, the pseudo-ductility was computed resorting on the following equation:

$$\mu = \frac{\gamma_u}{\gamma_y} \tag{3}$$

In Table 6, one can see the values of the pseudo-ductility for all the tested masonry panels.

An important observation that can be pointed out is that applying fiber reinforced mortar in the mortar joints enhances more the pseudo-ductility than when it is applied as external coating (the reader is referred to a comparison between the cases J-G_{FRM} and J-B_{FRM} with C-G_{FRM} and C-B_{FRM}). For one-head masonry panels, the best improvement in terms of pseudo-ductility corresponds to J-G_{FRM} and J-B_{FRM} cases, corresponding to cases of application of fiber reinforced mortar in both the joints and as an internal-external coating. For all cases, the best performance is shown by basalt fibers with respect to glass fibers. In fact,

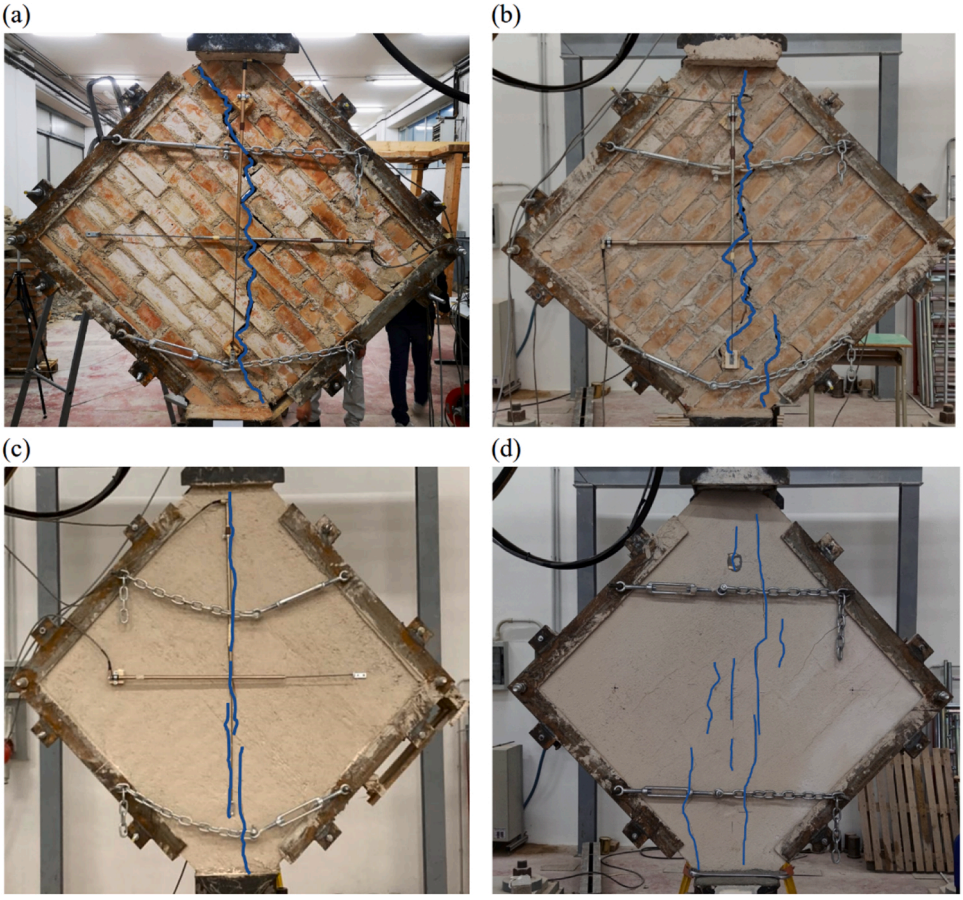

Fig. 8. Fracturing pattern for cases with reinforced mortar placed in: (a) mortar joints; (b) as internal-external coating; (c) both mortar joints and internal-external coating.

Table 6
Shear modulus, Young's modulus and Pseudo-ductility for all the tested masonry panels.

Nomenclature	Yield strain γ_y	Ultimate strain γ_u	Pseudo-ductility μ
URM	0.00075	0.0010	1.33
J-G_{FRM}	0.0025	0.0038	1.52
J-B_{FRM}	0.0020	0.0041	2.05
C_{URM}	0.0017	0.0019	1.12
C-G_{FRM}	0.0030	0.0042	1.40
C-B_{FRM}	0.0023	0.0039	1.70
JC-G_{FRM}	0.0022	0.0050	2.27
JC-B_{FRM}	0.0024	0.0065	2.70

μ related to J-G_{FRM}, C-G_{FRM} and JC-G_{FRM} cases is always lower than the one relate to the J-B_{FRM}, C-B_{FRM} and JC-B_{FRM} cases.

4. Conclusions

This paper studies the effect of basalt and fiber reinforced mortar on the compressive-shear behavior of one-head brick masonry panels. The fiber reinforced mortar is placed in three different locations with respect to the masonry walls: (i) in the mortar joints between bricks, (ii) on both external surfaces of the masonry panel, but joints were made out of plain mortar; (iii) both within the mortar joints and on the external surfaces of the panel.

The obtained results suggest to draw the following conclusions:

- using the fiber mortar within the mortar joints is moderately effective: panel shear strength enhances of about 67% and 48% (for basalt and glass fiber reinforced mortar, respectively) when compared to the unreinforced case
- using the fiber mortar as a double coating is moderately-highly effective: panel shear strength augments of about 249% and 129% (for basalt and glass fiber reinforced mortar, respectively) with respect to unreinforced case
- using the fiber mortar within the joints and as an internal-external coating highly effective: the panel shear strengths increase of about 329% and 286% (for basalt and glass fiber reinforced mortar, respectively) with respect to unreinforced case
- the reinforcement is more effective when located in the coating, for both basalt and glass fibers
- using the fiber reinforced mortar has a beneficial effect on the post-peak capacity: if fibers are used in the mortar joints the pseudo-ductility increases of about 14% and 54% (for glass and basalt fiber reinforced mortar, respectively); if fiber mortar is used as reinforcement of the external surfaced the pseudo-ductility augments of about 5% and 28%; when both of this reinforcement strategy are used contemporaneously, the pseudo-ductility enhances of about 70% and 103%.
- basalt fibers are always more effective than glass ones, for the enhancement of both the strength and the post-peak capacity

Overall, authors always advice to use chopped fiber reinforced mortar as strengthening system of new and existing masonry structures, above all when they are located in areas characterized by seismic hazard.

CRediT authorship contribution statement

Amedeo Gregori: Investigation, Project administration, Resources. **Micaela Mercuri:** Conceptualization, Data curation, Formal analysis, Investigation, Methodology, Project administration, Validation, Visualization, Writing – original draft, Writing – review & editing. **Marco Vailati:** Conceptualization, Data curation, Formal analysis, Methodology, Supervision, Validation, Writing – review & editing.

Declaration of Competing Interest

The authors declare that they have no known competing financial interests or personal relationships that could have appeared to influence the work reported in this paper.

Acknowledgement

The authors would also thank technicians Edoardo Ciuffitelli and Alfredo Peditto of the Laboratory of Material and Structures of University of L'Aquila.

References

[1] Mercuri M, Pathirage M, Gregori A, Cusatis G. On the collapse of the masonry Medici tower: An integrated discrete-analytical approach. Eng Struct 2021;246:113046.
[2] Mercuri M, Pathirage M, Gregori A, Cusatis G. Analysis of the behavior of the masonry Medici tower resorting on a hybrid discrete-kinematic methodology. Procedia Struct Integr 2023;44:1640–7.
[3] Vailati, M., Monti, G., Khazna, M.J., Napoli, A., & Realfonzo, R. (2012, September). Probabilistic assessment of masonry building clusters. In Proceedings of the 15th WCEE-World Conference of Earthquake Engineering (p. 1).
[4] Lagomarsino S. On the vulnerability assessment of monumental buildings. Bull Earthq Eng 2006;4:445–63.
[5] Feilden BM, Jokilehto J. Management guidelines for world cultural heritage sites. 1998. Hist Cities: Issues Urban Conserv 2019;8:425.
[6] Lagomarsino S, Podestà S. Damage and vulnerability assessment of churches after the 2002 Molise, Italy, earthquake. Earthq Spectra 2004;20(1_suppl):271–83.
[7] Mercuri M, Pathirage M, Gregori A, Cusatis G. Masonry vaulted structures under spreading supports: Analyses of fracturing behavior and size effect. J Build Eng 2022;45:103396.
[8] Mercuri M, Pathirage M, Gregori A, Cusatis G. Fracturing and collapse behavior of masonry vaulted structures: a lattice-discrete approach. Procedia Struct Integr 2023;44:1276–83.
[9] Mercuri M, Pathirage M, Gregori A, Cusatis G. Influence of self-weight on size effect of quasi-brittle materials: Generalized analytical formulation and application to the failure of irregular masonry arches. Int J Fract 2023:1–28.
[10] Gregori A, Mercuri M, Angiolilli M, Pathirage M. Simulating defects in brick masonry panels subjected to compressive loads. Eng Struct 2022;263:114333.
[11] Vailati M, Gregori A, Mercuri M, Monti G. A non-intrusive seismic retrofitting technique for masonry infills based on bed-joint sliding. J Build Eng 2023;69:106208.
[12] Vailati M, Monti G. Low-LOD fragility curves of structural units in masonry building clusters for territorial risk analysis. Eng Struct 2023;286:116143.
[13] Vailati M, Di Gangi G, Quaranta G. Thermo-mechanical characterization and hysteretic behavior identification of innovative plastic joint for masonry infills in reinforced concrete buildings. J Build Eng 2023;65:105803.
[14] Simões AG, Bento R, Lagomarsino S, Cattari S, Lourenço PB. Seismic assessment of nineteenth and twentieth centuries URM buildings in Lisbon: structural features and derivation of fragility curves. Bull Earthq Eng 2020;18:645–72.
[15] Triantafillou TC. Strengthening of masonry structures using epoxy-bonded FRP laminates. J Compos Constr 1998;2(2):96–104.
[16] Valluzzi MR, Tinazzi D, Modena C. Shear behavior of masonry panels strengthened by FRP laminates. Constr Build Mater 2002;16(7):409–16.
[17] Tumialan, J.G., Micelli, F., & Nanni, A. (2001). Strengthening of masonry structures with FRP composites. In Structures 2001: A Structural Engineering Odyssey (pp. 1–8).
[18] Carloni C, Subramaniam KV. FRP-masonry debonding: numerical and experimental study of the role of mortar joints. J Compos Constr 2012;16(5):581–9.
[19] Foraboschi P. Effectiveness of novel methods to increase the FRP-masonry bond capacity. Compos Part B: Eng 2016;107:214–32.
[20] Grande E, Milani G, Sacco E. Modelling and analysis of FRP-strengthened masonry panels. Eng Struct 2008;30(7):1842–60.
[21] Marcari G, Manfredi G, Prota A, Pecce M. In-plane shear performance of masonry panels strengthened with FRP. Compos Part B: Eng 2007;38(7-8):887–901.
[22] D'Ambrisi A, Feo L, Focacci F. Experimental and analytical investigation on bond between Carbon-FRCM materials and masonry. Compos Part B: Eng 2013;46:15–20.
[23] Carozzi FG, Milani G, Poggi C. Mechanical properties and numerical modeling of Fabric Reinforced Cementitious Matrix (FRCM) systems for strengthening of masonry structures. Compos Struct 2014;107:711–25.
[24] Maddaloni G, Cascardi A, Balsamo A, Di Ludovico M, Micelli F, Aiello MA, Prota A. Confinement of full-scale masonry columns with FRCM systems. Key engineering materials, Vol. 747. Trans Tech Publications Ltd,; 2017. p. 374–81.
[25] Bellini A, Incerti A, Bovo M, Mazzotti C. Effectiveness of FRCM reinforcement applied to masonry walls subject to axial force and out-of-plane loads evaluated by experimental and numerical studies. Int J Archit Herit 2018;12(3):376–94.
[26] D'Ambra C, Lignola GP, Prota A. Simple method to evaluate FRCM strengthening effects on in-plane shear capacity of masonry walls. Constr Build Mater 2021;268:121125.

[27] Ferretti F, Mazzotti C. FRCM/SRG strengthened masonry in diagonal compression: experimental results and analytical approach proposal. Constr Build Mater 2021; 283:122766.
[28] Castori G, Corradi M, Sperazini E. Full size testing and detailed micro-modeling of the in-plane behavior of FRCM–reinforced masonry. Constr Build Mater 2021;299: 124276.
[29] de Carvalho Bello CB, Cecchi A, Meroi E, Oliveira DV. Experimental and numerical investigations on the behaviour of masonry walls reinforced with an innovative sisal FRCM system. Key Engineering Materials, Vol. 747. Trans Tech Publications Ltd,; 2017. p. 190–5.
[30] Del Zoppo M, Di Ludovico M, Balsamo A, Prota A. Diagonal compression testing of masonry panels with irregular texture strengthened with inorganic composites. Mater Struct 2020;53:1–17.
[31] Mezrea PE, Ispir M, Balci IA, Bal IE, Ilki A. Diagonal tensile tests on historical brick masonry wallets strengthened with fabric reinforced cementitious mortar. Structures, Vol. 33. Elsevier,; 2021. p. 935–46.
[32] Casacci S, Gentilini C, Di Tommaso A, Oliveira DV. Shear strengthening of masonry wallettes resorting to structural repointing and FRCM composites. Constr Build Mater 2019;206:19–34.
[33] Garcia-Ramonda L, Pela L, Roca P, Camata G. In-plane shear behaviour by diagonal compression testing of brick masonry walls strengthened with basalt and steel textile reinforced mortars. Constr Build Mater 2020;240:117905.
[34] Crisci G, Ceroni F, Lignola GP. Efficiency of FRCM systems for strengthening of masonry walls. AIP Conference Proceedings, Vol. 2293. AIP Publishing LLC,; 2020, 240008.
[35] Babaeidarabad S, De Caso F, Nanni A. URM walls strengthened with fabric-reinforced cementitious matrix composite subjected to diagonal compression. J Compos Constr 2014;18(2):04013045.
[36] Segura J, Pelà L, Saloustros S, Roca P. Experimental and numerical insights on the diagonal compression test for the shear characterisation of masonry. Constr Build Mater 2021;287:122964.
[37] Codispoti R, Oliveira DV, Olivito RS, Lourenço PB, Fangueiro R. Mechanical performance of natural fiber-reinforced composites for the strengthening of masonry. Compos Part B: Eng 2015;77:74–83.
[38] Ismail, N., El-Maaddawy, T., Najmal, A., & Khattak, N. (2017, January). Diagonal tension testing of as-built and fabric reinforced cementitious matrix strengthened masonry panels. In Proceedings of the 16th World Conference of Earthquake Engineering.
[39] Mercedes L, Bernat-Maso E, Gil L. In-plane cyclic loading of masonry walls strengthened by vegetal-fabric-reinforced cementitious matrix (FRCM) composites. Eng Struct 2020;221:111097.
[40] Shabdin M, Zargaran M, Attari NK. Experimental diagonal tension (shear) test of Un-Reinforced Masonry (URM) walls strengthened with textile reinforced mortar (TRM). Constr Build Mater 2018;164:704–15.
[41] Incerti A, Tilocca AR, Bellini A, Savoia M. In-plane behaviour of FRCM-strengthened masonry panels. Brick and Block Masonry-From Historical to Sustainable Masonry. CRC Press,; 2020. p. 313–21.
[42] Incerti, A., Ferretti, F., & Mazzotti, C. (2018). Influence of FRCM retrofitting systems on the shear behaviour of pre-damaged masonry panels. In Proc. 10th Int. Mason. Soc. Conf. Milan (pp. 2240–9).
[43] Bertolesi E, Milani G, Poggi C. Simple holonomic homogenization model for the non-linear static analysis of in-plane loaded masonry walls strengthened with FRCM composites. Compos Struct 2016;158:291–307.
[44] Cucuzza R, Domaneschi M, Camata G, Marano GC, Formisano A, Brigante D. FRCM retrofitting techniques for masonry walls: a literature review and some laboratory tests. Procedia Struct Integr 2023;44:2190–7.
[45] Ferretti F, Khatiwada S, Incerti A, Giacomin G, Tomaro F, De Martino V, Mazzotti C. Structural strengthening of masonry elements by reinforced repointing combined with FRCM and CRM. Procedia Struct Integr 2023;44:2254–61.
[46] Mazzotti C, Ferretti F, Ferracuti B, Incerti A. Diagonal compression tests on masonry panels strengthened by FRP and FRCM. Structural analysis of historical constructions: Anamnesis, diagnosis, therapy, controls. CRC Press,; 2016. p. 1069–76.
[47] D'Antino T, Carozzi FG, Poggi C. Diagonal compression of masonry walls strengthened with composite reinforced mortar. Key Engineering Materials, Vol. 817. Trans Tech Publications Ltd,; 2019. p. 528–35.
[48] Sagar SL, Singhal V, Rai DC, Gudur P. Diagonal shear and out-of-plane flexural strength of fabric-reinforced cementitious matrix–strengthened masonry walletes. J Compos Constr 2017;21(4):04017016.
[49] Babaeidarabad S, Nanni A. In-plane behavior of unreinforced masonry walls strengthened with fabric-reinforced cementitious matrix (FRCM). Acids Spec Publ 2015;299:69–80.
[50] Crisci G, Ceroni F, Lignola GP. Comparison between design formulations and numerical results for in-plane FRCM-strengthened masonry walls. Appl Sci 2020;10 (14):4998.
[51] Del Zoppo M, Di Ludovico M, Balsamo A, Prota A. Experimental in-plane shear capacity of clay brick masonry panels strengthened with FRCM and FRM composites. J Compos Constr 2019;23(5):04019038.
[52] D'Ambra C, Lignola GP, Prota A, Fabbrocino F, Sacco E. FRCM strengthening of clay brick walls for out of plane loads. Compos Part B: Eng 2019;174:107050.
[53] Ismail, N., El-Maaddawy, T., Khattak, N., Walsh, K.Q., & Ingham, J.M. (2018, July). Out-of-plane behaviour of in-plane damaged masonry infills strengthened using fibre reinforced matrix. In 10th International Masonry Conference (pp. 9–11).
[54] Mercuri M, Pathirage M, Gregori A, Cusatis G. Computational modeling of the out-of-plane behavior of unreinforced irregular masonry. Eng Struct 2020;223:111181.
[55] Mercuri, M., Pathirage, M., Gregori, A., & Cusatis, G. (2021). Lattice discrete modeling of out-of-plane behavior of irregular masonry. In Proceedings of the 8th ECCOMAS Thematic Conference on Computational Methods in Structural Dynamics and Earthquake Engineering (pp. 546–562).
[56] Scacco J, Ghiassi B, Milani G, Lourenço PB. A fast modeling approach for numerical analysis of unreinforced and FRCM reinforced masonry walls under out-of-plane loading. Compos Part B: Eng 2020;180:107553.
[57] D'Antino T, Carozzi FG, Colombi P, Poggi C. Out-of-plane maximum resisting bending moment of masonry walls strengthened with FRCM composites. Compos Struct 2018;202:881–96.
[58] Bellini A, Incerti A, Bovo M, Mazzotti C. Effectiveness of FRCM reinforcement applied to masonry walls subject to axial force and out-of-plane loads evaluated by experimental and numerical studies. Int J Archit Herit 2018;12(3):376–94.
[59] De Santis, S., De Canio, G., de Felice, G., Meriggi, P., & Roselli, I. Out-of-plane seismic retrofitting of masonry walls with Textile Reinforced Mortar composites. Bull Earthq Eng 2019;17(11):6265–300.
[60] Meriggi P, de Felice G, De Santis S. Design of the out-of-plane strengthening of masonry walls with fabric reinforced cementitious matrix composites. Constr Build Mater 2020;240:117946.
[61] Bisby, L., Stratford, T., Hart, C., & Farren, S. (2013). Fire performance of well-anchored TRM, FRCM and FRP flexural strengthening systems. Advanced Composites in Construction; Network Group for Composites in Construction: Chesterfield, UK, 113.
[62] Swamy RN, Bahia HM. The effectiveness of steel fibers as shear reinforcement. Concr Int 1985;7(3):35–40.
[63] Maage M. Interaction between steel fibers and cement based matrixes. Matér Et Constr 1977;10:297–301.
[64] Sneed LH, Verre S, Carloni C, Ombres L. Flexural behavior of RC beams strengthened with steel-FRCM composite. Eng Struct 2016;127:686–99.
[65] Ombres, L., & Verre, S. (2018). Masonry columns strengthened with Steel Fabric Reinforced Cementitious Matrix (S-FRCM) jackets: Experimental and numerical analysis. Measurement, 127, 238–245.
[66] Morgan P. Carbon Fibers and their Composites. CRC Press,; 2005.
[67] Faleschini F, Zanini MA, Hofer L, Pellegrino C. Experimental behavior of reinforced concrete columns confined with carbon-FRCM composites. Constr Build Mater 2020;243:118296.
[68] Carozzi FG, Bellini A, D'Antino T, de Felice G, Focacci F, Hojdys Ł, Poggi C. Experimental investigation of tensile and bond properties of Carbon-FRCM composites for strengthening masonry elements. Compos Part B: Eng 2017;128: 100–19.
[69] D'Ambrisi A, Focacci F, Luciano R, Alecci V, De Stefano M. Carbon-FRCM materials for structural upgrade of masonry arch road bridges. Compos Part B: Eng 2015;75: 355–66.
[70] D'Antino T, Poggi C. Stress redistribution in glass fibers of G-FRCM composites. Key Engineering Materials, Vol. 817. Trans Tech Publications Ltd,; 2019. p. 520–7.
[71] Žmindák M, Dudinský M. Computational modelling of composite materials reinforced by glass fibers. Procedia Eng 2012;48:701–10.
[72] D'Antino T, Pellegrino C, Carloni C, Sneed LH, Giacomin G. Experimental analysis of the bond behavior of glass, carbon, and steel FRCM composites. Key engineering materials, Vol. 624. Trans Tech Publications Ltd,; 2015. p. 371–8.
[73] Donnini J, Chiappini G, Lancioni G, Corinaldesi V. Tensile behaviour of glass FRCM systems with fabrics' overlap: Experimental results and numerical modeling. Compos Struct 2019;212:398–411.
[74] Ralegaonkar R, Gavali H, Aswath P, Abolmaali S. Application of chopped basalt fibers in reinforced mortar: A review. Constr Build Mater 2018;164:589–602.
[75] Jiang CH, McCarthy TJ, Chen D, Dong QQ. Influence of basalt fiber on performance of cement mortar. Key Engineering Materials, Vol. 426. Trans Tech Publications Ltd,; 2010. p. 93–6.
[76] Chen H, Xie C, Fu C, Liu J, Wei X, Wu D. Orthogonal Analysis on Mechanical Properties of Basalt–Polypropylene Fiber Mortar. Materials 2020;13(13):2937.
[77] Pehlivan AO. Investigation of fracture parameters of concrete incorporating basalt fibers. Rev Romana De Mater 2021;51(2):247–55.
[78] Palme, J. (2014). Investigation of the Addition of Basalt Fibres into Cement.
[79] Caggegi C, Carozzi FG, De Santis S, Fabbrocino F, Focacci F, Hojdys Ł, Zuccarino L. Experimental analysis on tensile and bond properties of PBO and aramid fabric reinforced cementitious matrix for strengthening masonry structures. Compos Part B: Eng 2017;127:175–95.
[80] de Carvalho Bello CB, Boem I, Cecchi A, Gattesco N, Oliveira DV. Experimental tests for the characterization of sisal fiber reinforced cementitious matrix for strengthening masonry structures. Constr Build Mater 2019;219:44–55.
[81] Cristaldi G, Latteri A, Recca G, Cicala G. Composites based on natural fibre fabrics. Woven Fabr Eng 2010;17:317–42.
[82] Vailati M, Mercuri M, Angiolilli M, Gregori A. Natural-fibrous lime-based mortar for the rapid retrofitting of heritage masonry buildings. Fibers 2021;9(11):68.
[83] EN B. 771-1: 2011+ A1: 2015 Specification for masonry units—Clay masonry units. London, UK: British Standards Institution,; 2015.
[84] EN 1015–11. (1999). Methods of test for mortar for masonry–Part 11: Determination of flexural and compressive strength of hardened mortar.
[85] Mercuri M, Vailati M, Gregori A. Lime-based mortar reinforced with randomly oriented polyvinyl-alcohol (PVA) fibers for strengthening historical masonry structures. Dev Built Environ 2023;14:100152.
[86] Borri A, Castori G, Corradi M, Speranzini E. Shear behavior of unreinforced and reinforced masonry panels subjected to in situ diagonal compression tests. Constr Build Mater 2011;25(12):4403–14.

[87] American society for testing material - ASTM.. E519/ E519M. Standard Test Method For Diagonal Tension (Shear) In Masonry Assemblages. ASTM International,; 2021.
[88] Giberson MF. Two nonlinear beams with definitions of ductility. J Struct Div 1969; 95(2):137–57.
[89] Fardis MN. Capacity design: Early history. Earthq Eng Struct Dyn 2018;47(14): 2887–96.
[90] Magenes, G., & Penna, A. (2011, February). Seismic design and assessment of masonry buildings in Europe: recent research and code development issues. In Proceedings of the 9th Australasian masonry conference (Vol. 15, p. 18). Queenstown, New Zealand: Australian Masonry Conference, Auckland. [80] Ismail, N., Petersen, R. B., Masia, M.